Sensing Static Forces with Free-Falling Nanoparticles

Erik Hebestreit, Martin Frimmer, René Reimann, and Lukas Novotny*
Photonics Laboratory, ETH Zürich, 8093 Zürich, Switzerland

(Received 30 December 2017; revised manuscript received 13 May 2018; published 7 August 2018)

Miniaturized mechanical sensors rely on resonant operation schemes, unsuited to detect static forces. We demonstrate a nanomechanical sensor for static forces based on an optically trapped nanoparticle in vacuum. Our technique relies on an off-resonant interaction of the particle with a weak static force, and a resonant readout of the displacement caused by this interaction. We demonstrate a sensitivity of 10 aN to static gravitational and electric forces. Our work provides a tool for the closer investigation of short-range forces, and marks an important step towards the realization of matter-wave interferometry with macroscopic objects.

DOI: 10.1103/PhysRevLett.121.063602

Despite our solid understanding of physics at both macroscopic and atomic scales, mesoscopic systems still bear countless secrets [1,2], such as Casimir and van der Waals forces [3], or possible corrections to our understanding of gravity [4]. The astounding force sensitivities of systems based on trapped atoms and matter-wave interferometers have led to groundbreaking experiments investigating these notoriously elusive effects [5–7]. In recent years, nanomechanics has matured to a state where it can complement trapped-atom-based systems [8–12]. While nanomechanical sensors cannot rival atom-based systems regarding ultimate force sensitivity, their large mass density makes them a unique tool to investigate short-range interactions in largely unexplored regimes. In particular, levitated nanoparticles [13,14] have been suggested for exploring the boundary between Casimir and van der Waals descriptions of short-range interactions [15], and for testing models of non-Newtonian gravity [16].

Nanomechanical force sensors, including levitated particles, typically harness the sensor's intrinsic resonance to amplify the response to a perturbation [11,17]. This scheme implies a trade-off between measurement bandwidth and sensitivity, providing great sensitivity only for signals close to the resonance frequency [18]. In particular, resonant sensing fails for truly static forces and it has remained an open question how to exploit the benefits of resonant sensing schemes for the detection of static interactions.

In this Letter, we propose and demonstrate a force-sensing scheme that transfers the superior performance of resonant sensors to the realm of static interactions. We implement this static-force-sensing technique using an optically levitated nanoparticle, whose oscillation frequency can be adjusted by tuning the intensity of the trapping laser. In combination with the precise position measurement of levitated particles, we achieve a static-force sensitivity of 10 aN. We demonstrate our sensor performance by detecting the gravitational interaction between the levitated particle and the earth during a free fall, as well as the Coulomb force acting on a charged particle in an electric field.

The principle of our force-sensing scheme, illustrated in Figs. 1(a)–1(c), is inspired by atom thermometry techniques [19,20]. We prepare a particle in a harmonic optical potential with a low energy E_0. The potential is stiff enough to render the particle's displacement due to the static force (which is to be measured) negligible. Then, we turn off the

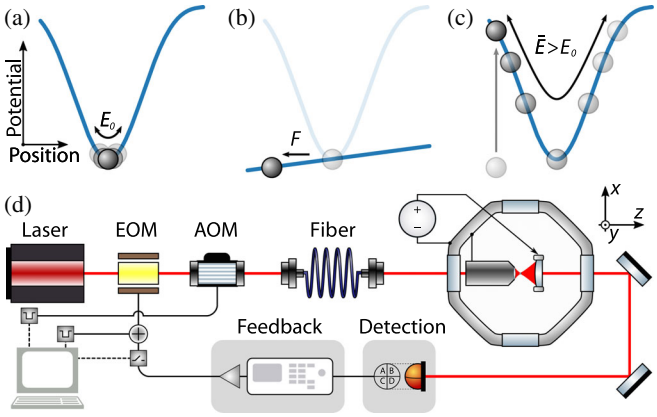

FIG. 1. (a) To initialize the system, we trap a nanoparticle with low energy E_0 in an optical potential (blue). (b) We deactivate the trapping potential for a time τ, during which the particle gets displaced by the static force F. (c) Upon reactivation of the optical trap, the particle gains potential energy due to its displacement from the trap center and oscillates with a higher amplitude than in (a). (d) Experimental setup. The nanoparticle is levitated in the focus of a laser beam inside a vacuum chamber. Gravity acts along the y axis. We switch the optical trap off with an electro- and acousto-optical modulator (EOM, AOM), measure the particle position with a balanced detector, and feedback cool the c.m. energy by modulating the trapping beam. Applying a voltage between the objective and the holder of the collection lens allows us to create a static electric field exerting a static force along the z axis on a charged particle.

trapping potential for an interaction time τ [see Fig. 1(b)]. The static force F displaces the particle, which upon reactivation of the potential results in an oscillation at the resonance frequency with an increased amplitude compared to the initial state [see Fig. 1(c)]. In the case of weak damping, we can measure this amplitude with high precision to deduce the magnitude of the static force.

Experimental setup.—A schematic of the experimental setup is shown in Fig. 1(d). We trap a silica nanosphere [nominal radius 58 nm, mass $m = 2.0(7)$ fg] in a strongly focused, linearly polarized laser beam (1064 nm, 140 mW, numerical aperture 0.85). The resulting oscillation frequencies of the particle are $\Omega_{z,0} = 2\pi \times 60$ kHz along the optical axis, and $\Omega_{x,0} = 2\pi \times 195$ kHz and $\Omega_{y,0} = 2\pi \times 160$ kHz in transverse directions. In this potential, a static force of 10 aN causes a displacement of merely 5 pm, which is both technically extremely challenging to detect and much smaller than any oscillation amplitude encountered in this work. Accordingly, we can neglect the influence of the static force in the presence of the trapping potential. Using intensity modulators, we can reduce the trapping power to below 100 nW, leading to typical optical forces below 0.2 aN, considerably weaker than the gravitational force between the particle and the Earth. To minimize interactions of the particle with the surrounding gas, we reduce the gas pressure below 10^{-5} mbar. Detecting the light scattered off the particle provides us with the particle's center-of-mass (c.m.) position [14]. We use this information to feedback cool the particle's c.m. motion to less than 100 mK [21]. To minimize possible electrostatic interactions with the environment, we discharge the nanoparticle prior to our experiment [22].

Measurement of gravitational force.—In a free-fall experiment, we measure the gravitational force $F = -mg = -20$ aN acting on the particle along the y axis. Figure 2(a) shows the protocol for a single free-fall cycle. First, we feedback cool the particle's c.m. energy. Second, at time $t = 0$, we switch off both the feedback and the optical trap, to allow the particle to freely interact with the gravitational force. Third, after the interaction time τ, we retrap the particle and observe its motion by switching the optical trap back on. In Fig. 2(b), we plot the c.m. motion along the y axis during one free-fall cycle at a pressure of 6×10^{-6} mbar. For $t < 0$, the c.m. energy is reduced to $E_{y,0}/k_B = 47$ mK [23]. From $t = 0$ to $t = \tau$, while the optical trap is deactivated, we have no information about the particle position (gray shaded area). For $t > \tau = 100$ μs, we observe a strongly underdamped oscillation of the particle at the trap frequency $\Omega_{y,0}$ (sinusoidal fit in orange). This large oscillation amplitude in the y direction originates from the displacement of the particle by the gravitational force [cf. Fig. 1(c)].

For comparison, we show in Fig. 2(c) the particle motion along the x axis, orthogonal to the direction of gravity, where no static force is acting. Before the free fall, we measure an initial c.m. energy of $E_{x,0}/k_B = 63$ mK. After the fall, we record an oscillation at the frequency $\Omega_{x,0}$ with an amplitude significantly larger than before the fall.

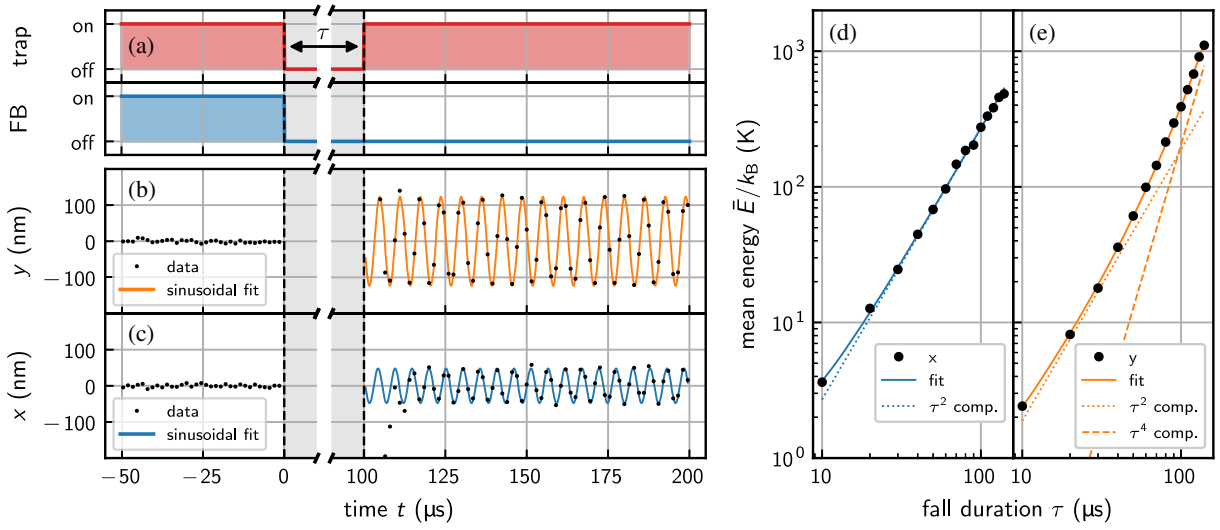

FIG. 2. (a) Timing scheme of a single free-fall cycle [cf. Figs. 1(a)–1(c)]. For $t < 0$, the trapping potential is on and the feedback (FB) cools the particle's c.m. motion. From $t = 0$ to $t = \tau = 100$ μs, we deactivate the optical trap and the feedback such that the particle can freely interact with the static force. At time $t = \tau$, the trap is reactivated while the feedback remains off. We plot the recorded motion along the y axis (b) and the x axis (c) in black. For $t > \tau$, the particle undergoes sinusoidal oscillations (orange and blue fit) with a larger amplitude along the y direction. (d) Average oscillation energy $\bar{E}$ after free fall in the x direction for varying fall durations τ (error bars are smaller than the symbol size). (e) Along the y axis, gravity accelerates the particle. For both axes, we fit $\bar{E} = \beta_0 + \beta_2\tau^2 + \beta_4\tau^4$ (solid line) and show the $\beta_2\tau^2$ term (dotted line), and the $\beta_4\tau^4$ term (dashed line). The latter only contributes for the y axis measurement, and is a signature of the gravitational acceleration.

At first sight, this observation seems to contradict our expectation in the absence of a static force. Indeed, for a particle that is at rest at time $t = 0$, we expect no oscillation after the free fall if no static force is acting. However, as the cooling is not perfect, the particle remains with a finite velocity $\dot{x}(0)$ at time $t = 0$, which leads to a displacement $\Delta x = \dot{x}(0)\tau$ directly after the fall.

Before the free fall, the feedback-cooled c.m. motion is in a thermal state, and the initial velocities $\dot{x}(0)$ and $\dot{y}(0)$ are therefore Gaussian distributed [21]. Accordingly, every iteration of the free-fall cycle results in a different oscillation amplitude after the fall. To estimate the expectation value of the c.m. energy, we integrate the power spectral density after the free fall over the oscillation peak Ω_0 for every one of the 1000 iterations, and average the measured c.m. energies [23]. We plot the mean c.m. energy for the horizontal x oscillation for varying fall durations between $\tau = 10$ μs and 140 μs in Fig. 2(d) as black dots. We find that the mean x oscillation energy scales quadratically with the fall duration τ (dotted line), which is expected as the initial velocity results in a displacement which is linear in time. In contrast, for the mean oscillation energy along the vertical y axis, shown in Fig. 2(e), we observe a significant deviation from this quadratic scaling for long fall durations, which originates from the gravitational acceleration of the particle.

To quantitatively understand the mean oscillation energy after the free fall, we study the evolution of the particle's phase-space distribution during the fall. The following derivation for the y axis remains equivalently valid for the other oscillation directions. For $t < 0$, the particle is in a thermal state with energy E_0. In position-velocity phase space, just before the free fall, this results in a Gaussian probability distribution

$$\mathcal{P}(y, \dot{y}; t = 0) = \frac{1}{Z} \exp\left(-\frac{m\Omega_0^2 y^2 + m\dot{y}^2}{2E_0}\right) \qquad (1)$$

that is centered at $y = \dot{y} = 0$ with $Z = 2\pi E_0/(m\Omega_0)$ [21]. In Fig. 3(a), we plot this theoretical phase-space distribution for an initial energy $E_0/k_B = 50$ mK and an oscillation frequency $\Omega_0 = 2\pi \times 160$ kHz.

During the free fall of duration τ, the particle's c.m. is accelerated by the static force F. The position at time $t = \tau$ becomes $y(\tau) = y(0) + \dot{y}(0)\tau + F\tau^2/(2m)$ and the velocity reads $\dot{y}(\tau) = \dot{y}(0) + F\tau/m$. In the absence of a force ($F = 0$), propagating Eq. (1) results in the phase-space distribution displayed in Fig. 3(b). The distribution spreads towards larger positions, because high initial velocities translate to large displacements after the fall. In the presence of a force $F = -20$ aN acting on the particle, the phase-space distribution from Fig. 3(b) is shifted towards negative positions and negative velocities [see Fig. 3(c)]. By integrating $\iint \mathcal{P}(y, \dot{y}; \tau) E(y, \dot{y}) dy d\dot{y}$ over the entire phase space, we derive the expectation value of the oscillation energy after the free fall [24]

$$\langle E \rangle(\tau) = E_0 + \frac{E_0\Omega_0^2}{2}\tau^2 + \frac{F^2}{2m}\tau^2 + \frac{F^2\Omega_0^2}{8m}\tau^4. \qquad (2)$$

The first term on the right-hand side of Eq. (2) is the initial c.m. energy, the second term is the potential energy originating from the displacement due to the initial velocity of the particle, and the last two terms are the kinetic and potential energy the particle acquires due to the static force. Note that for sufficiently long fall durations, the third term of Eq. (2) is negligible compared to the fourth term. Hence, a free evolution, in the absence of a force, results in a mean energy that scales quadratically with the fall duration τ, as observed in Fig. 2(d). In contrast, if a static force F is present, the mean oscillation energy scales with τ^4 for long fall durations, as observed in Fig. 2(e).

We fit $\bar{E} = \beta_0 + \beta_2\tau^2 + \beta_4\tau^4$ to the measured mean oscillation energies in Fig. 2(d) for the x and in Fig. 2(e) for the y axis (solid lines). First, using the fit parameter β_2, we derive the mean initial oscillation energy $E_0 = 2\beta_2/\Omega_0^2$, and find $E_{x,0}/k_B = 37(2)$ mK and $E_{y,0}/k_B = 37(2)$ mK. Second, we deduce the force that acts on the particle during the free fall $|F_y| = \sqrt{8m\beta_4/\Omega_0^2} = [21.2 \pm 0.5(\text{stat}) \pm 3.7(\text{syst})]$ aN, and derive a gravitational acceleration $g = [10.4 \pm 0.2(\text{stat}) \pm 1.8(\text{syst})]$ m/s^2. Here, the statistical uncertainty (stat) arises from the thermal distribution of the initial state and the systematic uncertainty (syst) originates from the uncertainty in the particle mass. Despite this being a moderate acceleration sensitivity compared to atom-based sensors [5], extending our measurement scheme to nanogram particles [25] potentially leads to nano-g sensitivity. We carry out an alternative procedure to extract the force based on the analysis of the phase-space distribution in Ref. [26].

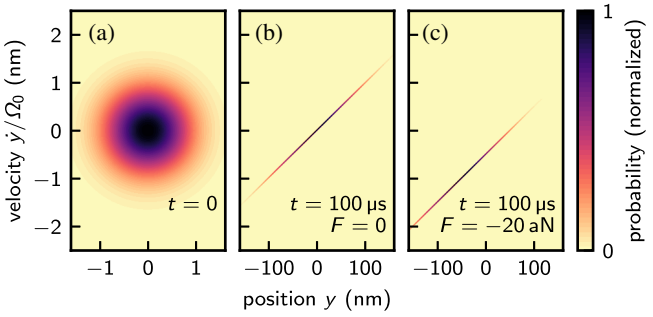

FIG. 3. Calculated phase-space distributions. (a) Initial probability distribution in phase space, corresponding to time $t = 0$ in Figs. 2(a)–2(c), shown for a thermal state with a c.m. energy of $E_0/k_B = 50$ mK. (b) Directly after a free evolution of duration $\tau = 100$ μs with deactivated trapping potential and in the absence of any force, the distribution is spread along the position axis due to the initial velocity of the particle. (c) Phase-space distribution after the evolution of duration $\tau = 100$ μs in the presence of a static force $F = -20$ aN. Compared to (b), the distribution is displaced by $\Delta y = F\tau^2/(2m) = -49$ nm and $\Delta\dot{y} = F\tau/m = -0.98$ nm/μs.

Electrostatic-force measurement.—As a further demonstration, we apply our static-force-sensing technique to measure a Coulomb force. To this end, we adjust the net charge on the nanoparticle to a single elementary charge [22,29]. By applying a voltage of 1 V to a capacitor formed by the objective and the holder of the collection lens, we generate an electric field $\mathcal{E} = 135$ V/m along the z direction [17] [see inset Fig. 4(a)], which corresponds to an expected electrostatic force $F = 22$ aN [22]. In Fig. 4(a), we plot for varying interaction times τ the average oscillation energy in z direction from 1000 free-fall cycles (green squares). We find a clear τ^4 scaling for interaction times exceeding 50 μs, indicating a static force along the z axis. When we reduce the applied electric field to $\mathcal{E} = 68$ V/m [orange triangles in Fig. 4(a)], and to $\mathcal{E} = 0$ (blue triangles), the measured oscillation energy reduces. Surprisingly, even when the capacitor field is switched off ($\mathcal{E} = 0$), we still observe a clear τ^4 dependence of the mean oscillation energy, meaning that there is a residual field accelerating the charged particle. In contrast, for an uncharged particle, the mean oscillation energy scales as τ^2 (gray dots), which means that no force accelerates the particle. The residual field we measure with a charged particle can be explained by contact (Volta) potentials [30] and stray fields due to patch charges on close-by surfaces [31]. To estimate the residual field $\mathcal{E}_{\mathrm{res}}$, we plot the fitting parameter β_4 for the three field amplitudes in Fig. 4(b). By fitting a quadratic function (black) to the data points, we find a residual electric field $\mathcal{E}_{\mathrm{res}} = 452(13)$ V/m when the capacitor field is switched off corresponding to a residual force $F_{\mathrm{res}} = 72(2)$ aN. For the case where we apply a field $\mathcal{E} = 135$ V/m (blue), we deduce a force $F = \sqrt{8m\beta_4/\Omega_0^2} = 92(17)$ aN, which means that we measure an additional force acting on the particle of $[19 \pm 7(\mathrm{stat}) \pm 3(\mathrm{syst})]$ aN when applying the capacitor field, which agrees with the expected value.

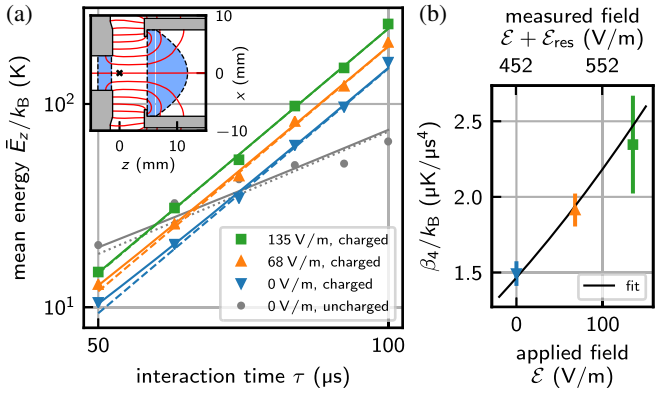

FIG. 4. (a) Mean energy in the z direction as a function of interaction time τ at different electric field strengths (squares and triangles). We fit $\bar{E} = \beta_0 + \beta_2\tau^2 + \beta_4\tau^4$ (solid lines) and indicate the $\beta_4\tau^4$ component of the fit (dashed) for the data taken with a charged particle. The energy of an uncharged particle (gray points) scales with τ^2 (dotted line, the initial energy is higher than in the charged case). Inset: Sketch of capacitor formed by objective and collection lens holder (metal gray, glass blue), and field lines (red). (b) Fitting parameters β_4 from (a) with $\beta_4(\mathcal{E}) = q^2(\mathcal{E} + \mathcal{E}_{\mathrm{res}})^2\Omega_0^2/(8m)$ (black). The deduced fitting parameter is the residual electric field strength $\mathcal{E}_{\mathrm{res}} = 452(13)$ V/m.

Discussion.—The sensitivity of our static-force measurement scheme scales as $\sqrt{E_0 m}/\tau$. It is limited by the energy E_0 of the particle before the fall, and by the interaction time τ (see Supplemental Material [26] for a detailed noise analysis). In the case of a mass-independent force F, our scheme benefits from a small particle mass and from the ability to efficiently cool the particle's c.m. energy [13,14]. Further improvements in the cooling performance to reach initial oscillation energies $E_0/k_B < 1$ mK are feasible, and even cooling to the quantum ground state of motion seems within reach [21]. For an initial energy of 1 mK, we estimate that the maximum interaction time τ is limited to ~300 μs by our ability to retrap the particle after the free fall, which would make the detection of static forces as low as 1 aN possible. For even longer interaction times, we envision a double-trap configuration to retrap the particle after the fall [32]. Alternatively, an electrostatic compensation of the gravitational force is possible using a suitable electrode configuration. For a ground-state cooled particle, we therefore estimate an ultimate limit of the interaction time of $\tau = 100$ ms, corresponding to a detection limit for static forces below 1 zN.

Conclusion.—We have demonstrated the measurement of a 10 aN static force using a levitated nanoparticle. Our technique is based on a free interaction of the particle with the static force while the trapping potential is deactivated, and a resonant readout of the subsequent oscillation. Because the particle's dynamics is measured along three orthogonal axes the scheme is applicable to the mapping of vectorial force fields. Our levitated nanoparticle sensor may be deployed for sensing short-range non-Newtonian forces by exploiting the particle's large mass density compared to atoms [16]. Furthermore, this high mass density paves the way towards the investigation of Casimir or van der Waals forces with an uncharged particle close to a surface [15]. Complementary to experiments with atoms [6,33], or macroscopic masses [34,35], nanoparticles allow the investigation of an unexplored intermediate regime of Casimir interactions, where the object size is comparable to the surface-object separation [15]. Together with recent work on optical levitation in close proximity of a dielectric surface, our free-fall scheme should allow resolving Casimir-Polder forces at separations smaller than 1 μm [36]. Importantly, in contrast to modulation-based schemes that are only sensitive to the surface-force gradient [33], our method provides access to the absolute value of the force. Finally, the demonstration of a controlled nanoparticle free-fall experiment marks an important step towards quantum-interference experiments and time-of-flight state tomography, which are essential building blocks for realizing non-Gaussian quantum states with macroscopic objects [37,38].

The authors acknowledge valuable discussions with Oriol Romero-Isart and Rozenn Diehl. This work has been supported by ERC-QMES (No. 338763) and the Swiss National Centre of Competence in Research (NCCR)—Quantum Science and Technology (QSIT) program (No. 51NF40-160591).

*www.photonics.ethz.ch

[1] R. H. French *et al.*, Rev. Mod. Phys. **82**, 1887 (2010).
[2] A. I. Volokitin and B. N. J. Persson, Rev. Mod. Phys. **79**, 1291 (2007).
[3] G. L. Klimchitskaya, U. Mohideen, and V. M. Mostepanenko, Rev. Mod. Phys. **81**, 1827 (2009).
[4] E. Fischbach and C. L. Talmadge, *The Search for Non-Newtonian Gravity* (Springer, New York, 1999).
[5] A. Peters, K. Y. Chung, and S. Chu, Nature (London) **400**, 849 (1999).
[6] J. M. Obrecht, R. J. Wild, M. Antezza, L. P. Pitaevskii, S. Stringari, and E. A. Cornell, Phys. Rev. Lett. **98**, 063201 (2007).
[7] H. Müller, S.-w. Chiow, S. Herrmann, S. Chu, and K.-Y. Chung, Phys. Rev. Lett. **100**, 031101 (2008).
[8] H. J. Mamin and D. Rugar, Appl. Phys. Lett. **79**, 3358 (2001).
[9] M. Li, H. X. Tang, and M. L. Roukes, Nat. Nanotechnol. **2**, 114 (2007).
[10] E. Gavartin, P. Verlot, and T. J. Kippenberg, Nat. Nanotechnol. **7**, 509 (2012).
[11] J. Moser, J. Güttinger, A. Eichler, M. J. Esplandiu, D. E. Liu, M. I. Dykman, and A. Bachtold, Nat. Nanotechnol. **8**, 493 (2013).
[12] R. A. Norte, J. P. Moura, and S. Gröblacher, Phys. Rev. Lett. **116**, 147202 (2016).
[13] T. Li, S. Kheifets, and M. G. Raizen, Nat. Phys. **7**, 527 (2011).
[14] J. Gieseler, B. Deutsch, R. Quidant, and L. Novotny, Phys. Rev. Lett. **109**, 103603 (2012).
[15] A. A. Geraci, S. B. Papp, and J. Kitching, Phys. Rev. Lett. **105**, 101101 (2010).
[16] A. Geraci and H. Goldman, Phys. Rev. D **92**, 062002 (2015).
[17] G. Ranjit, M. Cunningham, K. Casey, and A. A. Geraci, Phys. Rev. A **93**, 053801 (2016).
[18] V. Blūms, M. Piotrowski, M. I. Hussain, B. G. Norton, S. C. Connell, S. Gensemer, M. Lobino, and E. W. Streed, arXiv:1703.06561.
[19] S. Chu, L. Hollberg, J. E. Bjorkholm, A. Cable, and A. Ashkin, Phys. Rev. Lett. **55**, 48 (1985).
[20] M. Mudrich, S. Kraft, K. Singer, R. Grimm, A. Mosk, and M. Weidemüller, Phys. Rev. Lett. **88**, 253001 (2002).
[21] V. Jain, J. Gieseler, C. Moritz, C. Dellago, R. Quidant, and L. Novotny, Phys. Rev. Lett. **116**, 243601 (2016).
[22] M. Frimmer, K. Luszcz, S. Ferreiro, V. Jain, E. Hebestreit, and L. Novotny, Phys. Rev. A **95**, 061801 (2017).
[23] E. Hebestreit, M. Frimmer, R. Reimann, C. Dellago, F. Ricci, and L. Novotny, Rev. Sci. Instrum. **89**, 033111 (2018).
[24] S. M. Ross, *Introduction to Probability Models*, 11th ed. (Academic Press, Boston, Massachusetts, 2014).
[25] F. Monteiro, S. Ghosh, A. G. Fine, and D. C. Moore, Phys. Rev. A **96**, 063841 (2017).
[26] See Supplemental Material at http://link.aps.org/supplemental/10.1103/PhysRevLett.121.063602, for the reconstruction of the phase-space distribution, a signal-to-noise analysis, and the sensor response to harmonic forces, which includes Refs. [27,28].
[27] E. Hebestreit, M. Frimmer, R. Reimann, C. Dellago, F. Ricci, and L. Novotny, Rev. Sci. Instrum. **89**, 033111 (2018).
[28] M. Rashid, T. Tufarelli, J. Bateman, J. Vovrosh, D. Hempston, M. S. Kim, and H. Ulbricht, Phys. Rev. Lett. **117**, 273601 (2016).
[29] D. C. Moore, A. D. Rider, and G. Gratta, Phys. Rev. Lett. **113**, 251801 (2014).
[30] V. S. Bagotsky, *Fundamentals of Electrochemistry* (John Wiley & Sons, Inc., Hoboken, New Jersey, 2005).
[31] M. Brownnutt, M. Kumph, P. Rabl, and R. Blatt, Rev. Mod. Phys. **87**, 1419 (2015).
[32] L. Rondin, J. Gieseler, F. Ricci, R. Quidant, C. Dellago, and L. Novotny, Nat. Nanotechnol. **12**, 1130 (2017).
[33] C. I. Sukenik, M. G. Boshier, D. Cho, V. Sandoghdar, and E. A. Hinds, Phys. Rev. Lett. **70**, 560 (1993).
[34] S. K. Lamoreaux, Phys. Rev. Lett. **78**, 5 (1997).
[35] J. L. Garrett, D. A. T. Somers, and J. N. Munday, Phys. Rev. Lett. **120**, 040401 (2018).
[36] R. Diehl, E. Hebestreit, R. Reimann, M. Frimmer, F. Tebbenjohanns, and L. Novotny, Phys. Rev. A **98**, 013851 (2018).
[37] O. Romero-Isart, A. C. Pflanzer, M. L. Juan, R. Quidant, N. Kiesel, M. Aspelmeyer, and J. I. Cirac, Phys. Rev. A **83**, 013803 (2011).
[38] C. Wan, M. Scala, G. W. Morley, ATM. A. Rahman, H. Ulbricht, J. Bateman, P. F. Barker, S. Bose, and M. S. Kim, Phys. Rev. Lett. **117**, 143003 (2016).